Springer

Dear Author,

Here are the proofs of your article.

- You can submit your corrections **online**, via **e-mail** or by **fax**.

- For **online** submission please insert your corrections in the online correction form. Always indicate the line number to which the correction refers.

- You can also insert your corrections in the proof PDF and **email** the annotated PDF.

- For fax submission, please ensure that your corrections are clearly legible. Use a fine black pen and write the correction in the margin, not too close to the edge of the page.

- Remember to note the **journal title**, **article number**, and **your name** when sending your response via e-mail or fax.

- **Check** the metadata sheet to make sure that the header information, especially author names and the corresponding affiliations are correctly shown.

- **Check** the questions that may have arisen during copy editing and insert your answers/ corrections.

- **Check** that the text is complete and that all figures, tables and their legends are included. Also check the accuracy of special characters, equations, and electronic supplementary material if applicable. If necessary refer to the *Edited manuscript*.

- The publication of inaccurate data such as dosages and units can have serious consequences. Please take particular care that all such details are correct.

- Please **do not** make changes that involve only matters of style. We have generally introduced forms that follow the journal's style.
  Substantial changes in content, e.g., new results, corrected values, title and authorship are not allowed without the approval of the responsible editor. In such a case, please contact the Editorial Office and return his/her consent together with the proof.

- If we do not receive your corrections **within 48 hours**, we will send you a reminder.

- Your article will be published **Online First** approximately one week after receipt of your corrected proofs. This is the **official first publication** citable with the DOI. **Further changes are, therefore, not possible.**

- The **printed version** will follow in a forthcoming issue.

Please note

After online publication, subscribers (personal/institutional) to this journal will have access to the complete article via the DOI using the URL: http://dx.doi.org/[DOI].
If you would like to know when your article has been published online, take advantage of our free alert service. For registration and further information go to: http://www.link.springer.com.

Due to the electronic nature of the procedure, the manuscript and the original figures will only be returned to you on special request. When you return your corrections, please inform us if you would like to have these documents returned.

Metadata of the article that will be visualized in OnlineFirst

Corresponding Author	Family Name	**Sforza**
	Particle	
	Given Name	**Chiarella**
	Suffix	
	Division	Department of Biomedical Sciences for Health
	Organization	Università degli Studi di Milano
	Address	Milano, MI, 20133, Italy
	Email	chiarella.sforza@unimi.it
	ORCID	
Author	Family Name	**Codari**
	Particle	
	Given Name	**Marina**
	Suffix	
	Division	Department of Biomedical Sciences for Health
	Organization	Università degli Studi di Milano
	Address	Milano, MI, 20133, Italy
	Email	
	ORCID	
Author	Family Name	**Caffini**
	Particle	
	Given Name	**Matteo**
	Suffix	
	Division	
	Organization	CIMeC, Università degli Studi di Trento
	Address	Rovereto, TN, 38068, Italy
	Email	
	ORCID	
Author	Family Name	**Tartaglia**
	Particle	
	Given Name	**Gianluca M.**
	Suffix	
	Division	Department of Biomedical Sciences for Health
	Organization	Università degli Studi di Milano
	Address	Milano, MI, 20133, Italy
	Division	

	Organization	SST Dentofacial Clinic
	Address	Segrate, MI, 20090, Italy
	Email	
	ORCID	
Author	Family Name	**Baselli**
	Particle	
	Given Name	**Giuseppe**
	Suffix	
	Division	Department of Electronics, Information and Bioengineering
	Organization	Politecnico di Milano
	Address	Milano, MI, 20133, Italy
	Email	
	ORCID	

Abstract	*Purpose:*
	Nowadays, with the increased diffusion of Cone Beam Computerized Tomography (CBCT) scanners in dental and maxilla-facial practice, 3D cephalometric analysis is emerging. Maxillofacial surgeons and dentists make wide use of cephalometric analysis in diagnosis, surgery and treatment planning. Accuracy and repeatability of the manual approach, the most common approach in clinical practice, are limited by intra- and inter-subject variability in landmark identification. So, we propose a computer-aided landmark annotation approach that estimates the three-dimensional (3D) positions of 21 selected landmarks.
	Methods:
	The procedure involves an adaptive cluster-based segmentation of bone tissues followed by an intensity-based registration of an annotated reference volume onto a patient Cone Beam CT (CBCT) head volume. The outcomes of the annotation process are presented to the clinician as a 3D surface of the patient skull with the estimate landmark displayed on it. Moreover, each landmark is centered into a spherical confidence region that can help the clinician in a subsequent manual refinement of the annotation. The algorithm was validated onto 18 CBCT images.
	Results:
	Automatic segmentation shows a high accuracy level with no significant difference between automatically and manually determined threshold values. The overall median value of the localization error was equal to 1.99 mm with an interquartile range (IQR) of 1.22–2.89 mm.
	Conclusion:
	The obtained results are promising, segmentation was proved to be very robust and the achieved accuracy level in landmark annotation was acceptable for most of landmarks and comparable with other available methods.

Keywords (separated by '-')	Cone beam CT - Cephalometry - Image segmentation - Image registration
Footnote Information	

CrossMark

ORIGINAL ARTICLE

Computer-aided cephalometric landmark annotation for CBCT data

Marina Codari[1] · **Matteo Caffini[2]** · **Gianluca M. Tartaglia[1,3]** · **Chiarella Sforza[1]** · **Giuseppe Baselli[4]**

Abstract

Purpose Nowadays, with the increased diffusion of Cone Beam Computerized Tomography (CBCT) scanners in dental and maxilla-facial practice, 3D cephalometric analysis is emerging. Maxillofacial surgeons and dentists make wide use of cephalometric analysis in diagnosis, surgery and treatment planning. Accuracy and repeatability of the manual approach, the most common approach in clinical practice, are limited by intra- and inter-subject variability in landmark identification. So, we propose a computer-aided landmark annotation approach that estimates the three-dimensional (3D) positions of 21 selected landmarks.

Methods The procedure involves an adaptive cluster-based segmentation of bone tissues followed by an intensity-based registration of an annotated reference volume onto a patient Cone Beam CT (CBCT) head volume. The outcomes of the annotation process are presented to the clinician as a 3D surface of the patient skull with the estimate landmark displayed on it. Moreover, each landmark is centered into a spherical confidence region that can help the clinician in a subsequent manual refinement of the annotation. The algorithm was validated onto 18 CBCT images.

Results Automatic segmentation shows a high accuracy level with no significant difference between automatically and manually determined threshold values. The overall median value of the localization error was equal to 1.99 mm with an interquartile range (IQR) of 1.22–2.89 mm.

Conclusion The obtained results are promising, segmentation was proved to be very robust and the achieved accuracy level in landmark annotation was acceptable for most of landmarks and comparable with other available methods.

Keywords Cone beam CT · Cephalometry · Image segmentation · Image registration

✉ Chiarella Sforza
  chiarella.sforza@unimi.it

1 Department of Biomedical Sciences for Health, Università degli Studi di Milano, 20133 Milano, MI, Italy

2 CIMeC, Università degli Studi di Trento, 38068 Rovereto, TN, Italy

3 SST Dentofacial Clinic, 20090 Segrate, MI, Italy

4 Department of Electronics, Information and Bioengineering, Politecnico di Milano, 20133 Milano, MI, Italy

Introduction

The measurement of the head, known as cephalometry, considers both soft and hard tissues and has many applications in today's world. The application of cephalometry to the clinical needs, commonly known as cephalometric analysis, is widely used in dental applications, such as orthodontics and implantology, and in surgical planning and treatment evaluation for maxillofacial surgery [1–3]. Traditionally, cephalometric analyses have been manually performed on a 2D cephalogram, which is a standardized tracing of craniofacial structures as depicted by a latero-lateral radiography of the head. Currently, with the diffusion of Cone Beam Computerized Tomography (CBCT) scanners, 3D cephalometric analysis is emerging [4]. CBCT is used for small segments of the body, such as the head or part of it, and generally delivers lower dose to the patient, compared to CT [5]. In particular, CBCT is a useful tool for identification and evaluation of treatment outcomes, becoming one of the most common image modality used to visualize the facial skeleton [6–8]. Both maxillofacial surgeons and dentists can foresee remarkable developments by the aid of computerized methods permitting to easily extract individual features and perform measurements.

Nowadays, manual point-picking represents the method of choice to perform 3D cephalometric analysis; however, this approach is limited in accuracy and repeatability due to the differences in intra- and inter-operator landmark identification [9–11]. The need to overcome these limitations recently led to the development of aided, automated or nearly automated methods [12–18]. Here, we propose a semiautomatic computerized method that can help the clinician to annotate three-dimensional CBCT volumes of the human head, using intensity-based image registration.

Materials and methods

The proposed algorithm, entirely developed in MATLAB (MathWorks, Natick, MA, USA), automatically segments the skull from CBCT volumes of the human head and subsequently estimates a number of cephalometric landmarks. The flowchart of the proposed algorithm is presented in Fig. 1.

Anatomical landmarks

In this study, a set of fiducial points, which location will be estimated, must be decided and defined. To validate the proposed method, a set of 21 landmarks, commonly used in clinical practice and distributed all over the skull surface, was chosen [19]. All chosen landmarks and their definition are listed in Table 1 [20].

Dataset

Datasets of 18 subjects who underwent CBCT imaging examination at the SST Dentofacial Clinic, Italy, were retrospectively selected. These images were acquired for reasons independent of this study, and in all acquisitions, the device was operated at 6–10 mA (pulse mode) and 105 kV using a X-ray generator with fixed anode and 0.5 mm nominal focal spot size. All images were acquired with cephalometric field of view (200 mm × 170 mm). All subjects were adult healthy Caucasian women, aged from 37 to 74 years, who had teeth in both dental arches. No limitations was set to the presence of dental implants, dental fillings or even on particular dental treatments carried out before the radiological examination.

Image preprocessing

In order to standardize the structures in the CBCT data, the proposed method requires a single initialization step that consists in pointing the most inferior point of the mandibular bone. Currently, this is the only manual operation required; however, this is easy to automatize, provided a standard patient's positioning on the scanner chin set. Next, the volume is cut off below the selected slice and the algorithm proceeds automatically in landmarks' identification. This simple step defines a common criterion for volume limitation capable of providing a coarse standardization of the structures.
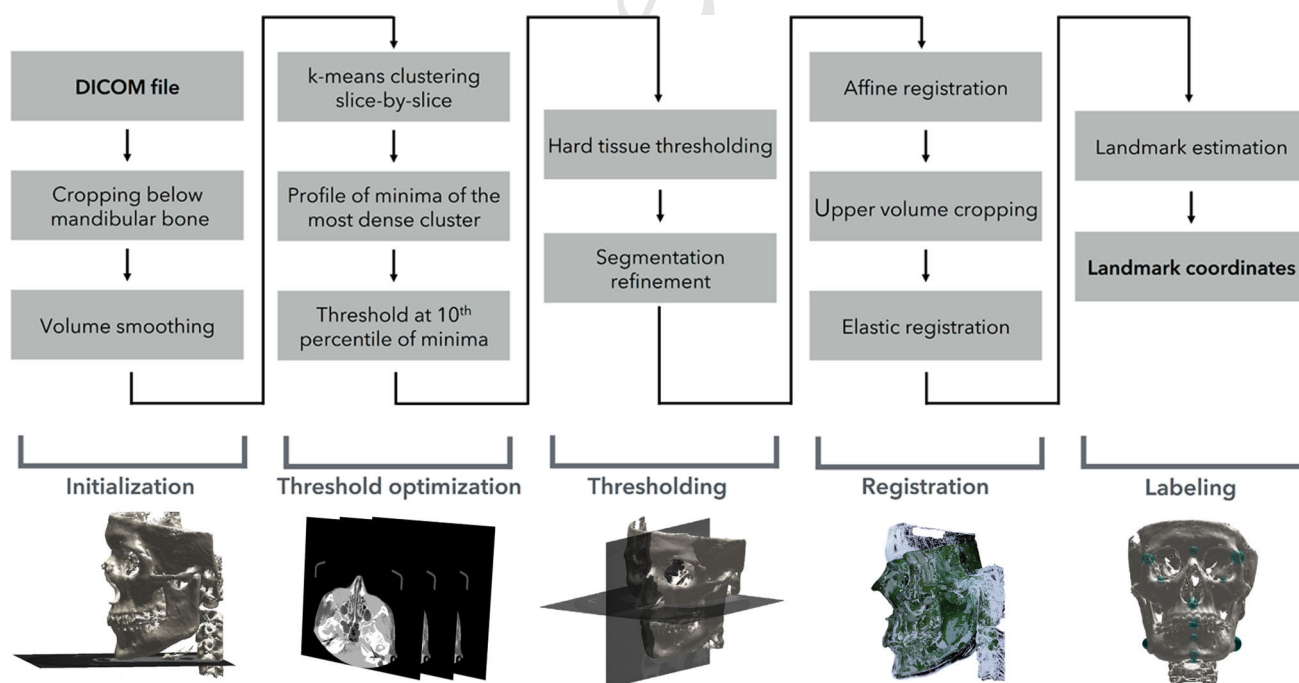

Fig. 1 Flowchart of the presented algorithm, which receives a DICOM file as input, articulates in 3 phases: image preprocessing, segmentation and registration and returns the landmark coordinates as output

Table 1 List of the 21 estimated landmarks as defined by Swennen et al. [16]

Landmark name	Abbreviation	Definition
Sella turcica	S	The center of the hypophyseal fossa
Nasion	N	The midpoint of the frontonasal suture
Left and right gonion	lGo and rGo	The point at each mandibular angle that is defined by dropping a perpendicular from the intersection point of the tangent lines to the posterior margin of the mandibular vertical ramus and inferior margin of the mandibular body or horizontal ramus
Anterior nasal spine	ANS	The most anterior midpoint of the anterior nasal spine of the maxilla
Pogonion	Pg	The most anterior midpoint of the chin on the outline of the mandibular symphysis
Menton	Me	The most inferior midpoint of the chin on the
Left and right orbitale	lOr	Outline of the mandibular symphysis
Posterior nasal spine	PNS	The most inferior point of each infraorbital rim
Left and right posterior maxillary points	lPM and rPM	The most posterior midpoint of the posterior nasal spine of the palatine bone
Left and right upper incisor	lUI and rUI	Is the most mesial point of the tip of the crown of each upper central incisor
Left and right lower incisor	lLI and rLI	Is the most mesial point of the tip of the crown of each lower central incisor
Frontozygomatic point	lFZ and rFZ	The most medial and anterior point of each frontozygomatic suture at the level of the lateral orbital rim
A point	A	The point of maximum concavity in the midline of the alveolar process of the maxilla
B point	B	Point of maximum concavity in the midline of the alveolar process of the mandible
Basion	Ba	The most anterior point of the great foramen

Subsequently, to improve the accuracy of the segmentation procedures and to make it robust to the presence of noise, the image was filtered using a three-dimensional low-pass Gaussian filter. The size of this cubic filter was set to 3 voxels in order to limit the blurring effect, increase signal-to-noise ratio and preserve the morphology of craniofacial bones [21].

Image segmentation

The segmentation algorithm aims at a standard hard tissue thresholding, though after a subject-specific adaptation with no manual interaction and no training dataset or previously developed models. A major consideration driving the algorithm design was that CBCT scanners provide less calibrated contrasts than CTs, thus reducing the confidence in preset thresholds [22].

This aim was approached by k-means clustering separately performed on a representative subset of the volume slices. In particular, the k-means clustering was chosen due to its low sensitivity to initialization parameters, relatively low computational complexity and its suitability for biomedical image segmentation since the number of clusters can be easily defined based on prior anatomical knowledge [23,24].

The present validation considered a 1:2 reduction, by analyzing each second slice; however, further preliminary trials revealed that higher reduction factors improved efficiency with no accuracy loss. As detailed below, the statistics of clusters was used to set the optimal soft/hard tissue separation threshold; also, a good robustness against dental metal artifacts was achieved by proper elimination of low-density outliers.

Within each subset, slice tissues were classified into 4 main categories, one representing air, two representing soft tissues and one representing hard tissues. The classification was performed using a k-means clustering approach [25]. The following statistics through the subset of slices considered the minimum of the highest intensity cluster; i.e., the one intended to classify bone and tooth tissue.

These values allowed to determine the global threshold which was defined at the 10th percentile of the population of minima. This threshold value was shown to make the algorithm robust to misclassification of tissues in a limited (i.e., less than 10 %) number of slices that are easily classified as outliers. The 10 % rule was selected to avoid a specific search of outliers.

After the optimized threshold value was obtained, it was possible to proceed with the thresholding of the entire volume that needs to be segmented, since preliminary analyses confirmed that possible intensity calibration trends through slices were negligible. The outcome of single-voxel thresholding was next improved by removing all the residual volumes of the segmentation process, caused by the presence of noise or artifacts. A 3D labeling process identified all structures, and those presenting a volume lower than 0.1 % of the total seg-
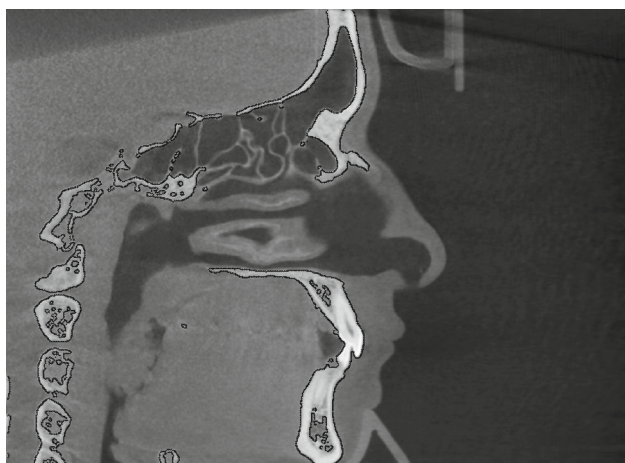
Fig. 2 The figure shows, in a median sagittal slice, which structures are maintained during the segmentation process

mented volume were eliminated. An example of the outcome of the segmentation process is shown in Fig. 2.

Image registration

Landmark placement was based on the propagation of landmarks through the registration on an annotated reference skull. The reference skull was automatically segmented with the above-presented method and annotated in a double-blind process by three expert operators for three times, in order to take intra- and inter-operator variability into account. Each operator had at least 4 years of experience in morphological evaluation of the skull. To allow the user to annotate the reference skull, a dedicated guided user interface (GUI) was created using MATLAB. This GUI allowed the user to annotate the skull visualizing multiplanar reconstruction (MPR) views. Once all the operators performed the annotation, the center of mass of all annotations was used as final landmark positions.

In previous investigations, deformable registration approaches have been used to align corresponding structures in different images in order to estimate anatomical landmarks, as such methods take into account the global appearance information of the anatomical structures [26–28]. During this step, segmentation for both subject and reference was used for masking only, thus keeping the information of gray levels inside the segmented bone. Registration was started by affine transformation that, being global and linear, permits rescaling according to the individual proportions and also allows a robust compensation of the different volumetric FOVs occurring in CBCT. Its transform is expressed by:

$$F : \mathbf{x}_F \in \Omega_F \rightarrow F(\mathbf{x}_F)$$

$$M : \mathbf{x}_M \in \Omega_M \rightarrow M(\mathbf{x}_M)$$

where $F(\mathbf{x}_F)$ is an intensity value of the image F at the location $\mathbf{x}_F$, Ω_F is the domain of the image F, $M(\mathbf{x}_M)$ is an intensity value of the image M at the location $\mathbf{x}_M$ and Ω_M is the domain of image M [15]. The mean squared intensity difference (MSD) was applied as registration objective function to be minimized. This cost figure is defined as follows:

$$MSD = \frac{1}{N} \sum_{\mathbf{x_F} \in \Omega_{F,M}^T} \left| F(\mathbf{x_F}) - M^{T_a}(\mathbf{x_M}) \right|^2 \tag{1}$$

where $\mathbf{x_F}$ represents the voxel locations in image F and $\Omega_{F,M}^T$ represents the overlap domain consisting of N voxel subset.

Trilinear interpolation was applied in computing the transformed image gray levels and an iterative gradient descent algorithm was applied to find the optimal transform:

$$R_a = M^{T_a} = T_a(M) \tag{2}$$

The affine registration (linear) step was used as initialization of a subsequent elastic registration (nonlinear). Importantly, the algorithm was designed to avoid deformations due to the presence of different anatomical structures in the image volumes, which were caused by the limited field of view of CBCT images and inter-subject morphological variability. This problem was solved by shrinking the subjects mask to the overlap subset $T_{F,M}$ found after the first affine registration step, thus cutting out the individual volume in excess to the reference volume. Then, the skulls were processed with a subsequent step of intensity-based global elastic registration, by MATLAB Medical Image Registration Toolbox, MIRT, Free Form Deformation (FFD) with three hierarchical levels of B-spline control points [30,31]. A wide mesh window size between the B-spline control points of 15 voxels was set, in order to register the main skull features while avoiding deformation relevant to the largely varying bone structure details and to artifacts. As a result, the number of control points varied for each image, depending on its size.

Moreover, in order to prevent the mesh to get too much deformed, a regularization term was used. In particular, the Euclidean distance between all the neighboring displacements of B-spline control points was penalized [30]. In our algorithm, the regularization weight was set to 0.1. Both mesh window size and regularization weight were empirically determined to give the best performance in term of accuracy.

Like the affine one, the elastic registration was an iterative process, which optimizes the MSD voxel similarity measure using a gradient descent optimization method with 3 hierarchical levels of optimization. This additional transformation T_e is defined as:

$$R_e = T_e(R_a) \tag{3}$$

An example of the outcome of these registration steps is depicted in Fig. 3, which shows how the elastic registration
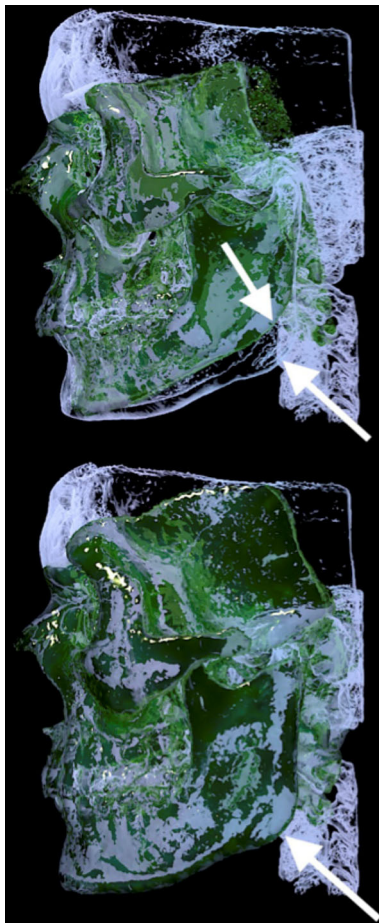
Fig. 3 Example of affine registration (*above*) and affine + elastic registration (*below*). Median sagittal view of the segmented subject skull (*light*) with the register

allowed to better adapt the morphology of the reference skull to the patient's one, compared to the affine step.

Landmark estimation

Through the registration phase, the algorithm superimposes and deforms the reference skull to comply with the morphology of the patient based on the intensity values of the segmented CBCT images. The combined transformations T_a and T_e can be readily applied to the coordinates of cephalometric landmarks annotated on the reference skull thus labeling the skull under examination.

Namely, the affine transformation T_a is described by a 4×4 matrix $\mathbf{T}_a$ (12 degrees of freedom) applied to the i-th landmark p_i ($i = 1, \ldots 21$) to obtain the landmark estimate in the patient's reference system, $\hat{p}_i^a$ [29]:

$$\hat{p}_i^a = T_a p_i \tag{4}$$

The elastic transformation T_e was implemented numerically on a zeros volume, the size of the original volume, marked with a single 1 at the landmark position. The transformed image was no more binary, and the center of mass coordinates was taken as transformed landmark coordinates. The 21 landmark coordinates were collected in a vector $\hat{p}_e$ representing the final estimation of the chosen cephalometric landmark coordinates.

At the end of the annotation process, each annotated landmark is displayed on the 3D surface of the patient skull. Moreover, each landmark is centered into a spherical confidence region that helps the clinician during a subsequent eventual manual refinement of the annotation, as can be seen in Fig. 4. The radius of the confidence spheres was set to the 95th percentile of the annotation error population calculated during the validation step.

Validation

Optimized thresholding, though preliminary to registration and automated annotation, was considered a crucial step deserving a specific validation. Therefore, the algorithm outcomes were compared to the manual thresholding performed by an experienced user on the whole data set. Both threshold values and segmented volumes were compared testing correlation and significance of differences of automatic vs. manual identification. Depending on the normality of data, either Student's *t* test or Wilcoxon signed-rank test was used; *p* value significance level was set to 0.05. The normality of data distribution was checked with Jarque-Bera test; also in this case significance level was set to 0.05.

To evaluate the quality of the annotations performed in this study, all CBCT volumes were manually annotated. In particular, in order to take the inter-operator variability of the annotation process into account, a team of expert users manually annotated the image dataset. This way, for each subject, the expected location of the 21 cephalometric landmarks can be defined as the barycenter of the operators' annotation. Fig. 4 shows an example of manually and automatically annotated landmarks.

Subsequently, the Euclidean distance, expressed in mm, between the position of each manually annotated landmark and the position of its corresponding landmark estimated by the proposed algorithm, was calculated. These distances will be subsequently used to display confidence regions around the estimate landmarks in order to allow the user to easily place the landmark in the most suitable place.

Results

Segmentation

To evaluate the accuracy of the segmentation process, both threshold values and segmented volumes were compared.
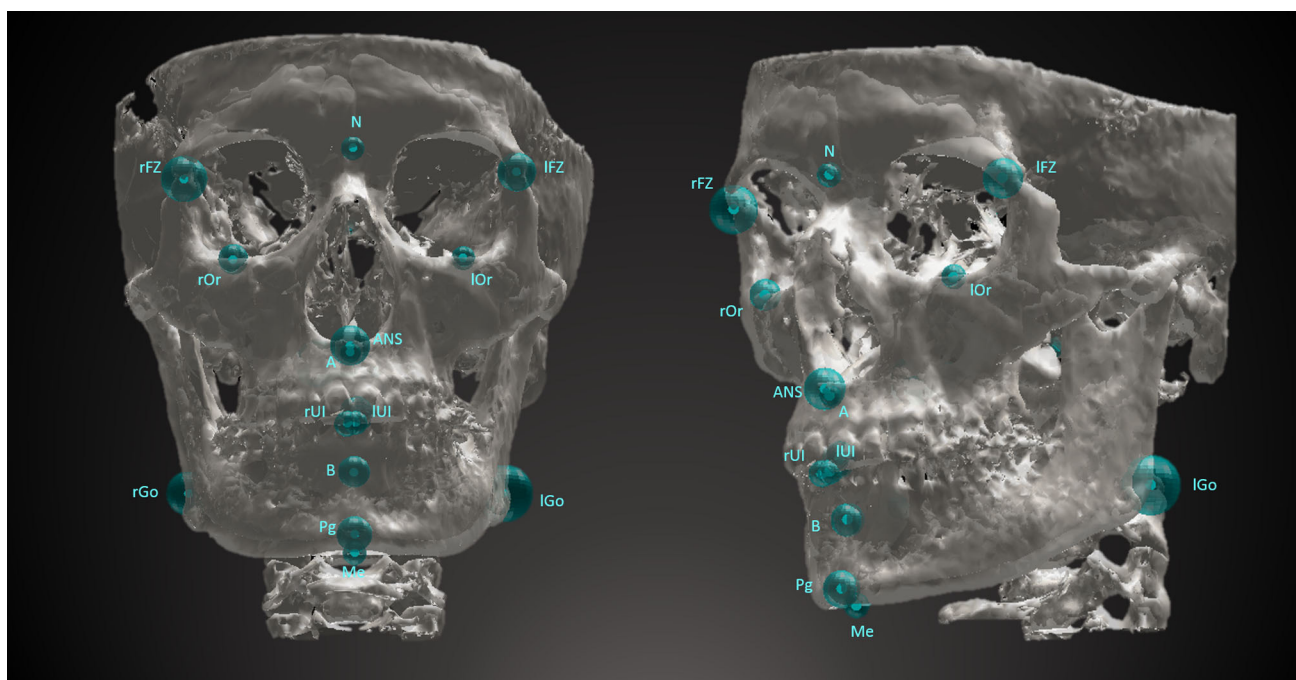
Fig. 4 Example of the proposed, computer-aided, annotation process outcome; each landmark is cantered into a spherical confidence region (95th percentile of the annotation error population) that can help the clinician in a subsequent manual refinement of the annotation

Both manual and automatic threshold values resulted normally distributed ($p > 0.05$). They were highly correlated ($R = 0.96$, $p < 0.001$), and no significant difference was found between them ($p > 0.05$), thus indicating that the automatic optimization well reproduced the threshold setting of experts.

Segmented volume values resulted not normally distributed ($p < 0.05$), and nonparametric tests were used for their statistical comparisons. Even for these values, a high level of accuracy was found between automatically and manually segmented volume values ($\rho = 0.98$, $p < 0.001$) and no significant differences were found between the two groups ($p > 0.05$).

Landmark estimation

The mean (standard deviation) inter-operator interclass correlation coefficient (ICC) for all the analyzed landmarks was 0.98 (0.04).

The overall median value of the computer-aided localization error was equal to 1.99 mm with an interquartile range (IQR) of 1.22–2.89 mm. This median error expressed in the horizontal, vertical and transverse direction was equal to 0.60, 0.86 and 0.89 mm, respectively. These distances widely varied among different landmarks. In particular, among the calculated estimation errors the lowest value was reported for the PNS landmark with a median value of 1.47 mm and an IQR of 0.79–1.76 mm. On the other hand, the highest values were observed for Gonia, respectively, right Gonion with a median value of 2.81 mm and an IQR of 1.46–4.83 mm and left Gonion with a median value of 4.00 mm and an IQR of 2.00–4.86 mm.

Considering all landmarks, annotation error was less than 5.00 mm for 90 % of landmarks and less than 2.50 mm for 63 % of them. The descriptive statistics for the obtained distances for each landmark are shown in Table 2.

Conclusion

The proposed method allows to find a good estimate of landmark positions, which may subsequently be refined by the clinician, saving operator time and reducing annotation variability.

Nowadays, the annotation of cephalometric points is mainly performed manually. Recent studies reported that the error caused by identification of landmark varies between 0.02 and 2.47 mm [9–11,32]. Therefore, one important aim for the evaluation of skeletal morphology in maxillofacial patients is to reduce the landmark identification error below 2.00 mm [32].

In the present study, landmarks lying in different locations present largely different average localization errors. Using our method, Gonia arise as the most difficult markers to localize. As a matter of fact, this reflects the variability of human anatomy and manual annotation. The mandibular bone, statistically, is among the most variable bones of the

Table 2 Descriptive statistics of the obtained Euclidean distances for each landmark

Landmark	Median [mm]	IQR [mm]	Max [mm]	Min [mm]
S	1.42	0.82–1.73	3.53	0.60
N	2.27	1.20–2.92	4.71	0.28
lGo	4.00	2.00–4.86	8.33	0.45
rGo	2.81	1.46–4.83	6.62	0.28
ANS	2.35	1.74–2.97	5.70	0.60
Pg	2.87	2.11–4.05	5.24	0.00
Me	1.61	1.36–2.09	3.60	0.30
lOr	1.47	0.89–2.23	4.46	0.28
rOr	1.34	0.83–2.27	5.20	0.30
PNS	1.47	0.79–1.76	4.62	0.30
lPM	1.61	1.09–2.41	3.63	0.50
rPM	1.97	1.25–2.93	7.26	0.69
lUI	1.40	0.95–2.05	3.60	0.37
rUI	2.01	1.39–2.40	7.27	0.82
lLI	2.19	1.68–2.58	3.89	1.04
rLI	3.07	2.22–3.92	5.84	0.92
lFZ	1.81	1.13–4.30	6.60	0.50
rFZ	2.01	1.31–2.94	6.98	0.82
A	1.73	1.04–2.35	3.68	0.69
B	2.83	1.64–3.68	5.31	0.73
Ba	2.22	1.68–2.67	2.98	1.08
All	1.99	1.22–2.89	8.33	0.0

skull [33], and this is reflected in the estimation of right and left Gonion [34].

In this study, since annotation errors were not normally distributed among different patients ($p < 0.001$), the median annotation error was used to access the process accuracy of the annotation process. In particular, the median annotation error was found as 1.99 mm with an IQR of 1.22–2.89 mm. In a recent study, Shahidi et al. validated an algorithm for landmark annotation based on 3D image registration for 14 landmarks on a dataset of 20 CBCT images. They obtained an overall mean error of 3.40 mm, which is significantly higher compared to the one obtained with the current method [16]. In another study, Gupta et al. proposed a knowledge-based algorithm for automatic detection of cephalometric landmarks on CBCT images that was validated on 30 CBCT images. Gupta et al. obtained a mean error of 2.01 mm with a standard deviation of 1.23 mm, which is comparable with the one obtained with the proposed methodology [18]. With our method, a comparable accuracy level was obtained with reduced *a priori* information about landmark positions.

The method described in the present study attempts a general and robust approach for the propagation of landmarks from an annotated reference skull to subject-specific ones. Due to the variability in skull morphology depending on gender, age and ethnicity, in this study we applied the proposed method to a specific category of patients: adult Caucasian women. To apply the same methodology on other patient categories, different atlases matched for sex, age and ethnicity must be used. The selection of only one specific sample represents a limitation of the current study but, at the same time, the low amount of a priori information needed from the proposed algorithm allows to test it on different patient categories simply changing the used atlas.

Segmentation of hard tissues is a fully automatic process that reduces the amount of error dependent on operator experience. In the validation step, no significant difference was found between manually and automatically determined threshold values. Moreover, the correlation coefficient close to 1 proved the high accuracy of the segmentation step compared to manual thresholding, which is now considered the standard method of segmentation in maxillofacial applications.

Since the segmentation step was proved to be very robust, the registration step represents the main source of variability in automatic annotation. In order to improve the annotation accuracy, local adaptation in a region of interest around each estimated landmark should be added to overcome the limits of the global registration step.

Moreover, we believe that a computer-aided cephalometric annotation of CBCT volumes, relying on intensity-based image registration, can be a good initialization that can help the clinician in performing cephalometric analysis. Indeed,

for most landmarks the current results are well comparable with those provided by other methods present in the literature [13,14]. One advantage of our method is that cephalometric landmark coordinates were obtained without any local a priori information about geometry and location of each landmark, allowing physicians to use this approach for personalized cephalometric analysis. Indeed, the method can be customized only changing the number of landmark annotated on the reference skull, without any modification of the annotation algorithm.

Results are promising; nevertheless, the study should be expanded in order to validate it on a larger dataset and reduce the estimation error to provide a fully automatic annotation algorithm. Moreover, in order to improve the segmentation and, consequently, the annotation in the dental region, a dedicated high intensity object artifact reducing algorithm should be implemented.

Compliance with ethical standards

Conflict of interest Marina Codari, Matteo Caffini, Chiarella Sforza, Gianluca M. Tartaglia and Giuseppe Baselli declare that they have no conflict of interest.

Staement of human rights For this type of study, formal consent is not required.

Informed consent Informed consent was obtained from all patients for being included in the study. The study was approved by the Institutional Review Board of the SST Dental Clinic (IRB03-2015 Doc. MQ 03 AL 02-MC).

References

1. Gateno J, Xia JJ, Teichgraeber JF (2011) New 3-dimensional cephalometric analysis for orthognathic surgery. J Oral Maxillofac Surg 69:606–622. doi:10.1016/j.joms.2010.09.010
2. Bettega G, Payan Y, Mollard B, Boyer A, Raphael B, Lavallèe S (2000) A simulator for maxillofacial surgery integrating 3D cephalometry and orthodontia. Comput Aided Surg 5:156–165
3. Hurst CA, Eppley BL, Havlik RJ, Sadove AM (2007) Surgical cephalometrics: applications and developments. Plast Reconstr Surg 120:92e–104e. doi:10.1097/01.prs.0000282728.97278.a2
4. Pittayapat P, Limchaichana-Bolstad N, Willems G, Jacobs R (2014) Three-dimensional cephalometric analysis in orthodontics: a systematic review. Orthod Craniofac Res 17:69–91. doi:10.1111/ocr.12034
5. Swennen GRJ, Schutyser F (2006) Three-dimensional cephalometry: spiral multi-slice vs cone-beam computed tomography. Am J Orthod Dentofacial Orthop 130:410–416. doi:10.1016/j.ajodo.2005.11.035
6. Al-Okshi A, Lindh C, Salé H, Gunnarsson M, Rohlin M (2015) Effective dose of cone beam CT (CBCT) of the facial skeleton: a systematic review. Br J Radiol 88:20140658. doi:10.1259/bjr.20140658
7. Weissheimer A, Menezes LM, Koerich L, Pham J, Cevidanes LHS (2015) Fast three-dimensional superimposition of cone beam computed tomography for orthopaedics and orthognathic surgery evaluation. Int J Oral Maxillofac Surg 44:1188–1196. doi:10.1016/j.ijom.2015.04.001
8. Sun Y, Luebbers H-T, Agbaje JO, Schepers S, Vrielinck L, Lambrichts I, Politis C (2013) Validation of anatomical landmarks-based registration for image-guided surgery: an in-vitro study. J Cranio-Maxillo-Facial Surg 41:522–526
9. Swennen GRJ, Schutyser F, Barth E-L, De Groeve P, De Mey A (2006) A new method of 3-D cephalometry part I: the anatomic cartesian 3-D reference system. J Craniofac Surg 17:314–325
10. Titiz I, Laubinger M, Keller T, Hertrich K, Hirschfelder U (2011) Repeatability and reproducibility of landmarks—a three-dimensional computed tomography study. Eur J Orthod 34:1–11. doi:10.1093/ejo/cjq190
11. Katkar RA, Kummet C, Dawson D, Moreno Uribe L, Allareddy V, Finkelstein M, Ruprecht A (2013) Comparison of observer reliability of three-dimensional cephalometric landmark identification on subject images from Galileos and i-CAT cone beam CT. Dentomaxillofacial Radiol 42:1–11. doi:10.1259/dmfr.20130059
12. Cheng Y, Leow WK (2012) Automatic identification of frankfurt plane and mid-sagittal plane of skull. IEEE Work Appl Comput Vis 2012:233–238. doi:10.1109/WACV.2012.6162994
13. Keustermans J, Mollemans W, Vandermeulen D, Suetens P (2010) Automated cephalometric landmark identification using shape and local appearance models. In: IEEE 20th International conference on pattern recognition, pp 2464–2467
14. Keustermans J, Smeets D, Vandermeulen D, Suetens P (2011) Automated cephalometric landmark localization using sparse shape and appearance models. In: International workshop on machine learning medical imaging. Springer, Berlin Heidelberg, pp 249–256
15. Wang L, Chen KC, Gao Y, Shi F, Liao S, Li G, Shen SGF, Yan J, Lee PKM, Chow B, Liu NX, Xia JJ, Shen D (2014) Automated bone segmentation from dental CBCT images using patch-based sparse representation and convex optimization. Med Phys 41:043503. doi:10.1118/1.4868455
16. Shahidi S, Bahrampour E, Soltanimehr E, Zamani A, Oshagh M, Moattari M, Mehdizadeh A (2014) The accuracy of a designed software for automated localization of craniofacial landmarks on CBCT images. BMC Med Imaging 14:32. doi:10.1186/1471-2342-14-32
17. Makram M, Kamel H (2014) Reeb graph for automatic 3D cephalometry. Int J Image Process 8:17–29
18. Gupta A, Kharbanda OP, Sardana V, Balachandran R, Sardana HK (2015) A knowledge-based algorithm for automatic detection of cephalometric landmarks on CBCT images. Int J Comput Assist Radiol Surg 10:1737–1752. doi:10.1007/s11548-015-1173-6
19. de Oliveira AEF, Cevidanes LHS, Phillips C, Motta A, Burke B, Tyndall D (2009) Observer reliability of three-dimensional cephalometric landmark identification on cone-beam computerized tomography. Oral Surg Oral Med Oral Pathol Oral Radiol Endod 107:256–265. doi:10.1016/j.tripleo.2008.05.039
20. Swennen GRJ, Schutyser F, Hausamen JE (2005) Three-dimensional cephalometry: a color atlas and manual. Springer Science & Business Media, Berlin
21. Sagawa M, Miyoseta Y, Hayakawa Y, Honda A (2009) Comparison of two- and three-dimensional filtering methods to improve image quality in multiplanar reconstruction of cone-beam computed tomography. Oral Radiol 25:154–158. doi:10.1007/s11282-009-0026-9
22. Hassan B, Souza PC, Jacobs R, de Azambuja Berti S, van der Stelt P (2010) Influence of scanning and reconstruction parameters on quality of three-dimensional surface models of the dental arches from cone beam computed tomography. Clin Oral Investig 14:303–310. doi:10.1007/s00784-009-0291-3
23. Pham DL, Xu C, Prince JL (2000) Current methods in medical image segmentation 1. Annu Rev Biomed Eng 2:315–337
24. Ng HP, Ong SH, Foong KWC, Goh PS, Nowinski WL (2006) Medical image segmentation using K-means clustering and improved

watershed algorithm. In: 2006 IEEE southwest symposium on image analysis and interpretation pp 61–65

25. MacKay DJ (2003) Information theory, inference and learning algorithms. Cambridge University Press, Cambridge

26. Gao Y, Zhan Y, Shen D (2014) Incremental learning with selective memory (ILSM): towards fast prostate localization for image guided radiotherapy yaozong. IEEE Trans Med Imaging 33:518–534. doi:10.1109/TMI.2013.2291495

27. Liu J, Gao W, Huang S, Nowinski WL (2008) A model-based, semi-global segmentation approach for automatic 3-D point landmark localization in neuroimages. IEEE Trans Med Imaging 27:1034–1044. doi:10.1109/TMI.2008.915684

28. Frantz S, Rohr K, Stiehl HS (2000) Localization of 3D anatomical point landmarks in 3D tomographic images using deformable models. In: International conference on medical image computing and computer-assisted intervention 2000. Springer Berlin Heidelberg, pp 492–501

29. Hill DL, Batchelor PG, Holden M, Hawkes DJ (2001) Medical image registration. Phys Med Biol 46:R1–R45

30. Myronenko A, Song X (2010) Intensity-based image registration by minimizing residual complexity. IEEE Trans Med Imaging 29:1882–1891

31. Rueckert D, Sonoda LI, Hayes C, Hill DL, Leach MO, Hawkes DJ (1999) Nonrigid registration using free-form deformations: application to breast MR images. IEEE Trans Med Imaging 18:712–721. doi:10.1109/42.796284

32. Baan F, Liebregts J, Xi T, Schreurs R, de Koning M, Bergé S, Maal T (2016) A new 3D tool for assessing the accuracy of bimaxillary surgery: the orthognathic analyser. PLoS One 11:e0149625. doi:10.1371/journal.pone.0149625

33. Puisoru M, Forna N, Fatu A, Fuatu R, Fuatu C (2006) Analysis of mandibular variability in humans of different geographic areas. Ann Anatomy-Anatomischer Anzeiger 188:547–554

34. Schlicher W, Nielsen I, Huang JC, Maki K, Hatcher DC, Miller AJ (2012) Consistency and precision of landmark identification in three-dimensional cone beam computed tomography scans. Eur J Orthod 34:263–275. doi:10.1093/ejo/cjq144

Springer
the language of science

Author Query Form

**Please ensure you fill out your response to the queries raised below
and return this form along with your corrections**

Dear Author

During the process of typesetting your article, the following queries have arisen. Please check your typeset proof carefully against the queries listed below and mark the necessary changes either directly on the proof/online grid or in the 'Author's response' area provided below

Query	Details required	Author's response
1.	Please check the edit made in the article title.	
2.	Please check and confirm the edit made in reference Keustermans et al. (2010).	
3.	Please check and confirm the edit made in reference Keustermans et al. (2011).	
4.	Please check and confirm whether the inserted publisher location is correctly identified for the reference Swennen et al. (2005).	
5.	Please check and confirm the edit made in reference Ng et al. (2006).	
6.	Please check and confirm the edit made in reference Frantz et al. (2000).	